JOURNAL OF GEOPHYSICAL RESEARCH, VOL. 98, NO. D2, PAGES 2741–2745, FEBRUARY 20, 1993

The 200- to 300-nm Radiation Field in the Stratosphere: Comparison of Models With Observation

A. KYLLING AND K. STAMNES

Geophysical Institute, University of Alaska-Fairbanks, Fairbanks

R. R. MEIER

E. O. Hulburt, Center for Space Research, Space Science Division, Naval Research Laboratory, Washington, D. C.

D. E. ANDERSON

The Johns Hopkins University, Applied Physics Laboratory, Laurel, Maryland

The SABE 1 experiment (Herman and Mentall, 1982) measured the direct and scattered solar radiation at wavelengths between 190 and 320 nm from a balloon floating at 40 km altitude. We use state of the art radiative transfer models together with cross sections and solar flux data commonly used in modeling of the stratosphere to calculate the direct and scattered radiation at 40 km. The comparison between theory and experiment made by Herman and Mentall (1982) is extended. Significant discrepancies in the ratio of the scattered to direct flux not discussed in their work were found in the Schumann-Runge band and above 280 nm. Possible reasons for the differences are discussed.

1. INTRODUCTION

Knowledge of the UV and visible radiation field is essential for an understanding of photochemical processes in the troposphere and stratosphere. Remarkably, there are few actual observations. An attempt to remedy this situation was made by *Herman and Mentall* [1982, hereafter referred to as *HM*]. They observed the direct, attenuated solar ultraviolet radiation between 190 and 320 nm from both a rocket and a balloon, as well as the component of the radiation field produced by atmospheric scattering. The latter was measured for six directions in the sky from a balloon at 40 km. In general, models of the radiance were able to reproduce the observations (see Figure 8 of *HM*), although discrepancies were seen for certain directions (compare their Figures 5 and 6).

The Stratospheric Airborne Experiment (SABE 1) has long served as a reference of the radiation field in the upper stratosphere. It covers a wavelength region that is of great importance in photochemical modeling. As such it has provided modelers with data against which they may test their radiative models in the "relatively simple" case of Rayleigh scattering. Both above 300 nm and below 210 nm, multiple scattering can enhance the total radiation field. Comparisons of theoretical calculations and experiments may be used to assess our understanding of the atmospheric radiation field. Discrepancies between theory and experiments may indicate that our understanding of the "clear sky" radiation field is yet not complete.

The ratio of the scattered radiation to the direct, attenuated solar radiation provides a measure of the importance of multiple scattering. Here "direct attenuated radiation" refers to a plane perpendicular to the direction of the Sun (i.e., not the vertical), whereas the term "scattered radiation" is used to denote the diffuse sky radiation integrated over 4π steradians. In order to compute the ratio of the scattered to direct radiation in the stratosphere, hereafter referred to as the "scattering ratio," both the direct, attenuated solar radiation and the multiply scattered radiation must be known. *HM* obtained the latter by integrating the observed intensity over the sky, using an interpolation scheme for directions other than those of the measurements. Figure 11 of *HM* shows the observed scattering ratio between 200 and 310 nm (also reproduced in Figure 2 of the present paper). The multiply scattered radiation is less than 1% of the direct radiation near 250 nm but approaches 10% near both 200 and 300 nm. Comparison of the observed ratio to a theoretical ratio was not shown by *HM*, but with regard to the O_2 absorption cross sections they concluded that "on the basis of the measurements of the scattered flux within the Schumann-Runge band region of O_2 the effective cross sections used in current calculations need to be modified to allow greater penetration of the solar radiation into the atmosphere where scattering occurs." In this work we extend the comparison between theory and experiment made by *HM* and discuss important discrepancies not mentioned elsewhere.

In section 2 we give a brief description of the different radiation models employed in this work. The model results are presented and compared with the experimental results of *HM* in section 3. Finally, in section 4 we give our conclusion and recommendation for further research.

Paper number 92JD02687.
0148-0227/93/92JD-02687$05.00

2. MODEL DESCRIPTION

The scattered radiation measured by SABE 1 is 4π times the mean intensity

$$\overline{I(\tau)} = \frac{1}{4\pi}\int_0^{2\pi} d\phi \int_0^{\pi} I(\tau,\ \theta,\ \phi)\ \sin\theta\ d\theta$$

$$= \frac{1}{2}\int_{-1}^{1} I(\tau,\ \mu)\ d\mu \quad (1)$$

where the azimuthally averaged intensity is defined by

$$I(\tau,\ \mu) = \frac{1}{2\pi}\int_0^{2\pi} I(\tau,\ \mu,\ \phi)\ d\phi. \quad (2)$$

Here τ is the total (Rayleigh plus absorption) optical depth and θ ($\mu = \cos\theta$) and ϕ the polar and azimuthal angles, respectively. The direct radiation is described by the Lambert-Beer extinction law, whereas the azimuthally averaged diffuse intensity is governed by the radiative transfer equation

$$\frac{dI(\tau,\mu)}{d\tau} = I(\tau,\ \mu) - \frac{\omega(\tau)}{2}\int_{-1}^{1} p(\tau,\ \mu,\ \mu')I(\tau,\mu')\ d\mu'$$

$$- \frac{F_0}{4\pi}\,p(\tau, -\mu_0,\ \mu)e^{-\tau/\mu_0}. \quad (3)$$

The second term on the right-hand side is the multiple-scattering term. The scattering properties of the atmosphere are described by the phase function $p(\tau,\ \mu,\ \mu')$ and the single scattering albedo $\omega(\tau)$. The third term on the right-hand side is the direct beam source where F_0 is the solar flux (normal to the beam direction) at the top of the atmosphere incident at the angle μ_0. We note that the radiative transfer equation used in this work is linear in F_0. Hence when taking the ratio between the scattered and the direct radiation which both have the same source, the magnitude of the source cancels and only the optical properties of the medium matter. Thus the solar flux data have no effect on the scattering ratios calculated and measured.

We solved the radiative transfer equation (3) using the discrete ordinate algorithm of *Stamnes et al.* [1988]. An alternative approach developed at the Naval Research Laboratory (NRL) recasts the differential equation (3) into an integral equation, allowing solution for the ratio $\bar{I}/F_0$ directly, i.e., an integral equation solution of the radiative transfer equation for the mean intensity [*Anderson and Meier*, 1979; *Meier et al.*, 1982; *Anderson and Lloyd*, 1990]. This equation can be solved rapidly if isotropy is assumed for the Rayleigh-scattering phase function. A second NRL model was also developed using the Monte Carlo approach [*Anderson and Meier*, 1979]. Although the Monte Carlo model was computationally slower, it incorporated all relevant physical processes. Detailed comparisons of $\bar{I}/F_0$ computed with the two NRL models and the discrete ordinate model described above showed excellent agreement (less than 5% difference). The assumption of isotropic scattering invoked in the matrix inversion model led to errors of less than 5%. Since the discrete ordinate model is also computationally fast, is intrinsically accurate, and allows rapid computation of $I(\tau,\ \mu)$ for comparison with measured radiances, we have used it exclusively in this paper.

The accuracy of the discrete ordinate method depends on the number of quadrature points (or streams) used to approximate the integral in (3). All calculations presented in this paper where performed with a 16-stream model which is sufficient for the nearly isotropic Rayleigh scattering. To calculate the intensity at specific angles (other than the quadrature angles) and with high angular resolution (Figure 4) the interpolation scheme due to *Stamnes* [1982] was utilized.

TABLE 1. Atmospheric Profile Used in the Radiation Calculations

z, km	p, mbar	T, K	O_3, cm^{-3}
100.0	0.00032	190.0	5.00E + 07
95.0	0.00076	180.0	9.90E + 07
90.0	0.00184	173.0	1.50E + 08
85.0	0.00446	180.0	2.00E + 08
80.0	0.01050	190.0	2.20E + 08
75.0	0.02400	205.0	4.70E + 08
70.0	0.05220	220.0	1.30E + 09
65.0	0.10900	235.0	3.30E + 09
60.0	0.21900	250.0	7.07E + 09
55.0	0.42500	255.0	2.13E + 10
50.0	0.79780	257.0	6.62E + 10
47.5	1.09000	255.0	1.20E + 11
45.0	1.49100	253.0	2.15E + 11
44.0	1.69681	251.0	2.64E + 11
43.0	1.93103	250.6	3.24E + 11
42.0	2.20141	249.0	4.00E + 11
41.0	2.51401	247.0	4.92E + 11
40.0	2.87100	245.0	6.07E + 11
39.0	3.32690	243.0	7.31E + 11
38.0	3.85518	241.0	8.80E + 11
37.5	4.15000	240.0	9.65E + 11
35.0	5.74600	235.0	1.38E + 12
32.5	8.01000	232.0	1.86E + 12
30.0	11.97000	230.0	3.00E + 12
27.5	17.43000	225.0	3.60E + 12
25.0	25.49000	220.0	4.20E + 12
24.0	29.72000	218.0	3.84E + 12
23.0	34.67000	216.0	3.48E + 12
22.0	40.47000	214.0	3.12E + 12
21.0	47.29000	212.0	2.76E + 12
20.0	55.29000	210.0	2.40E + 12
19.0	64.67000	209.0	1.97E + 12
18.0	75.65000	207.7	1.54E + 12
17.0	88.50000	205.0	1.11E + 12
16.0	103.50000	206.0	6.88E + 11
15.0	121.10000	210.0	2.60E + 11
14.0	141.70000	216.0	2.36E + 11
13.0	165.80000	222.0	2.12E + 11
12.0	194.00000	228.0	1.88E + 11
11.0	227.00000	234.0	1.64E + 11
10.0	265.00000	240.0	1.40E + 11
9.0	308.00000	246.0	2.72E + 11
8.0	356.50000	252.0	4.04E + 11
7.0	411.10001	258.0	5.36E + 11
6.0	472.20001	264.0	6.68E + 11
5.0	540.50000	270.0	8.00E + 11
4.0	616.59998	276.0	8.20E + 11
3.0	701.20001	282.0	8.40E + 11
2.0	795.00000	288.0	8.60E + 11
1.0	898.79999	294.0	8.80E + 11
0.0	1013.00000	300.0	9.00E + 11

Read 5.00E + 7 as 5.00×10^7.

Atmospheric ozone and temperature profiles were taken from *Herman and Mentall* [1982]; see Table 1 and discussion below. The ozone absorption cross sections were taken from *Molina and Molina* [1986] and for the Rayleigh-scattering cross section we used the formula provided by *Nicolet* [1984]. For molecular oxygen we adopted the parameterization due to *Allen and Frederick* [1982] in the Schumann-Runge band, whereas in the Herzberg continuum we used values similar to those reported by *Shardanand and Pradad*

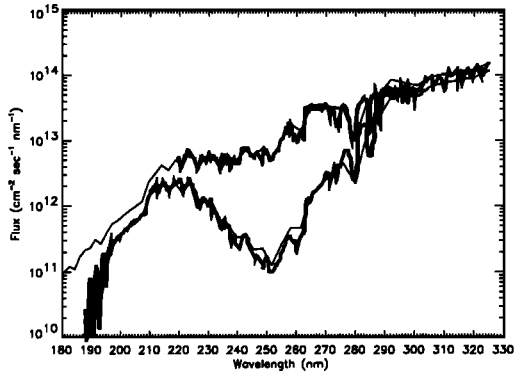

Fig. 1. The direct flux above the atmosphere and at 40 km altitude. The thin lines are the calculated fluxes, while the thick solid lines are experimental data taken from Figures 1 and 12 of *Herman and Mentall* (*HM*) [1982]. *HM* does not give values for the flux above the atmosphere for wavelengths shorter than 220 nm.

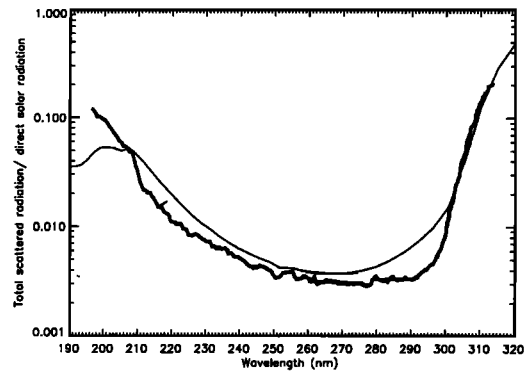

Fig. 2. The ratio of the scattered to the direct radiation at 40 km altitude. The thick solid line is the experimental curve of *HM*, their Figure 11, while the thin line represents model results.

Rao [1977] and corrected as suggested by *Frederick and Mentall* [1982]. The solar flux was taken from *World Meteorological Organization* (*WMO*) [1986] and modified to agree with the measurements of *HM* (Figure 1). All calculations were carried out with the wavelength resolution used in most photochemical models in this wavelength region: 190.5, 192.3, 194.2, 196.1, 198.0, 200.0, 202.0, 204.1, 206.2, 208.3, 210.5, 212.8, 215.0, 217.4, 219.8, 222.2, 224.7, 227.3, 229.9, 232.6, 235.3, 238.1, 241.0, 243.9, 246.9, 250.0, 253.2, 256.4, 259.7, 263.2, 266.7, 270.3, 274.0, 277.8, 281.7, 285.7, 289.9, 294.1, 298.5, 303.0, 307.7, 312.5, and 317.5 nm [*WMO*, 1986].

3. Model Results and Discussion

Our aim is to compute the ratio of the scattered radiation to the direct attenuated solar radiation and compare it to the ratio measured by the SABE 1 experiment. As a model atmosphere we adopted the profiles in Figure 10 of *HM*. We first calculated the direct downward flux at 40 km and compared it with the results of *HM*, as shown in Figure 1. The direct beam radiation is very sensitive to ozone content for wavelengths where ozone absorbs most strongly, i.e., around 255 nm, whereas in regions where the ozone absorption is small, changes in ozone content have little effect, as discussed by *HM*. Since the scattering ratio is the ratio of the scattered to the direct radiation, it is obviously important to calculate the direct radiation correctly. To reproduce the measured direct flux at 40 km, an altitude resolution of 1 km was required in the model atmosphere just above 40 km. A coarser resolution of 2.5 km used initially, underestimated the direct flux regardless of whether we assumed that the ozone density varied linearly or exponentially across a single layer. This was caused by an overestimation of the optical depth by the coarser resolution. In all calculations presented below, the ozone is assumed to vary linearly within each layer. The atmospheric profiles we used in the calculations are as given in Table 1 unless otherwise noted.

Our computed scattering ratio reproduces the main features of the measured scattering ratio, as shown in Figure 2. However, there are significant discrepancies. Between 210 and 300 nm the model predicts more scattering than the experiment. In particular, between 280 and 300 nm the model gives more scattering, up to a factor of 2, than inferred from the observations. Between 210 and 230 nm (part of the Herzberg continuum) the model also predicts more scattering than measured, whereas below 210 nm (Schumann-Runge bands) the measurements show more scattering. We note that there is a certain degree of symmetry in the differences around the wavelength of maximum ozone absorption, 255 nm.

HM estimate the experimental error in the scattering ratio to be ±10%. They do not give an error estimate of their data reduction method, i.e., the error made in deducing the mean intensity using information from only six directions. However, they estimate that their interpolation scheme gives a scattering ratio equal to or lower than the scattering actual ratio. If their measurements could be corrected for this the empirical and modeled scattering ratios would probably agree better. The difference in shape would still be present though. To test how sensitive the results are to the Rayleigh optical depth, we performed calculations in which the Rayleigh optical depth was changed by ±5%. Insignificant changes were observed in the scattered and direct radiation.

Lary and Pyle [1991] have also computed the scattering ratio and compared with *HM*. They conclude that their model agrees well with the measurements, even though they obtain a difference of more than a factor 3 below 200 nm. Our experience with the use of different ozone profiles in calculating the scattering ratio suggests that the shape of their modeled scattering ratio is caused by their ozone profile, which was "a standard atmospheric ozone profile" and not representative of the conditions encountered during the experiment of *HM*. We discuss below possible sources for the discrepancies between the experimental results and our model results.

Temperature effects. The temperature dependence of the ozone cross section is important above 280 nm [*Molina and Molina*, 1986]. Thus a different temperature profile will give a different curve for the scattering ratio. Between 280 and 300 nm the ozone absorption cross section varies roughly ±5% from $T = 226$ K to $T = 298$ K around its value at $T = 263$ K. We performed radiation calculations in which the temperature profile was shifted ±10 K. Such temperature changes do indeed produce different results for the scattering ratio. However, as the scattered radiation is driven by the direct beam radiation, increasing the latter will increase the former and their ratio will not change much, as our calculations showed. Thus for a realistic temperature profile, the temperature dependence measured by laboratory experiments in this wavelength region is too small to explain

the discrepancy between the observed and the computed scattering ratio.

Albedo effects. For the atmosphere model given in Table 1 and the solar elevation encountered during the experiment, the radiation penetrates to the ground for wavelengths larger than 292 nm, but only beyond 300 nm is enough radiation transmitted to make albedo effects important. We used the same albedo of 0.2 as was assumed by *HM*. Calculations were also performed with an albedo of 1.0. Although no significant change below 300 nm is found for the latter case, the experimental and theoretical scattering ratios are in better agreement above 300 nm. Experimental data beyond 320 nm would be of great value when studying albedo effects.

Polarization. Another possible source of error can be traced to polarization of the Rayleigh-scattered light. Although the models do not take polarization into account, the effect is expected to be small for computing sky-integrated intensities. However, the degree of polarization of the scattered intensities, which depends on the amount of multiple scattering, may result in an important effect. Below 300 nm, pure absorption prevents strong multiple scattering, so that intensities in specific directions may be significantly polarized. The observations of *HM* were made with spectrometers, whose throughput may be dependent on the polarization of the incident light (J. E. Mentall, private communication, 1983). Measurements of the polarization dependence of an 1/8-m Ebert-Fastie spectrometer by R. P. McCoy (private communication, 1991) have shown a response varying from 25 to 75% ($= (I_\perp - I_\parallel)/(I_\perp + I_\parallel)$) across the 200- to 300-nm range. The effects of neglecting polarization by *HM* are not clear. Good agreement between computed and observed intensities was found for certain directions (see Figure 8 of *HM*) but not for others (compare curves "5" of Figures 5 and 6 of *HM*).

Aerosols. Aerosols may significantly alter the optical properties of the atmosphere. Generally, the scattering and absorption properties of aerosols vary slowly with wavelength [*Shettle*, 1989; *Kylling*, 1992]. Thus plausible aerosol loadings do not provide an easy explanation of the strongly wavelength dependent difference between the measured and the modeled scattering ratio. An aerosol layer of volcanic origin has its maximum thickness typically around 20 km. The layer will increase the amount of scattered radiation above the cloud due to backscattering [*Kylling*, 1992]. Hence the scattering ratio will increase if aerosols are included in the model calculations and thus further increase the discrepancy between the empirical and the model results.

Schumann-Runge bands. The largest discrepancy between the measurement and the model occurs in the region of the Schumann-Runge bands. At 200 nm the ozone absorption cross section has a minimum. Less absorption above and below 40 km means more radiation available for scattering. At both sides of the minimum one would expect the scattering ratio to behave similarly. Hence more absorption means a lower scattering ratio, especially so below 200 nm where both ozone and the Schumann-Runge bands contribute to the absorption. This behavior of the scattering ratio is seen in the results from the present model but is absent in the empirical ratio curve of *HM*. The direct beam radiation displayed in Figure 1 of the present paper and Figure 12 of *HM* both exhibit this behavior due to increased absorption below 200 nm, as do the modeled scattered radiation field shown in Figure 3. However, the scattered radiation field

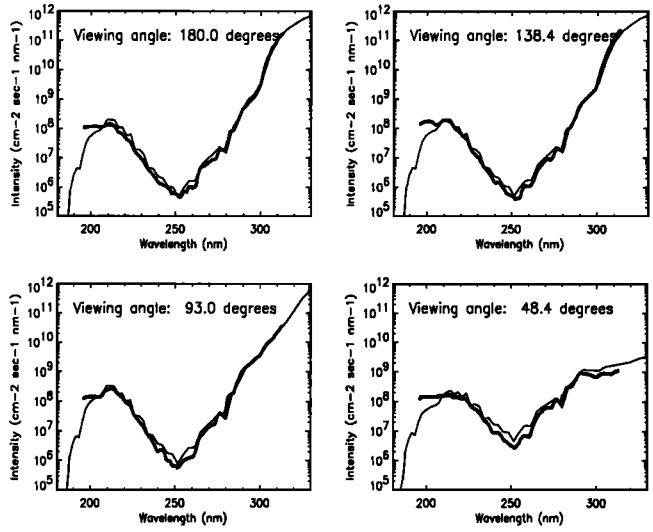

Fig. 3. The scattered solar radiation for four ($\theta = 180.0°$, $\theta = 138.4°$, $\theta = 93.0°$, and $\theta = 48.4°$) of the six viewing directions of the SABE 1 experiment (experimental data, thick lines). The angles are relative to the vertical with $\theta = 0°$ being in the zenith direction. The modeled data (thin lines) shown have been corrected to take into account the instrument aperture of 0.0474 steradians. To be compared with Figure 5 of *HM*.

measured by *HM* and shown in their Figure 5 does not exhibit this behavior. Since the scattered radiation field is driven by the direct beam radiation (Figure 12 of *HM*), one would expect that the direct and scattered radiation fields have a similar spectral shape. We note that calculations by *Luther and Gelinas* [1976], for a similar situation, show very little contribution from the scattered component to the total radiation in this wavelength region (their Figure 3*a*). *HM* suggest that the discrepancy seen in the highly structured Schumann-Runge bands may be due to the use of "bin-averaged" cross sections corresponding to the coarse wavelength resolution of the solar flux used as input. We may test this hypothesis by turning off all oxygen absorption in the model. This does bring the modeled scattering ratio somewhat closer to the measured one, but we are no longer able to reproduce the direct radiation curve given in Figure 12 of *HM* and Figure 1 of the present paper.

Altering the ozone column. The uniformity in the difference between the modeled and measured scattering ratio suggests that a change in the ozone content may alter the result. Above 40 km the ozone profile is constrained by the requirement that we must be able to reproduce the direct radiation at 40 km. A decrease in ozone below 40 km decreases absorption of radiation and leads to a higher scattering ratio, thus increasing the difference between the observed and the calculated scattering ratios. An increase in ozone below 40 km will increase the absorption and may thus lead to a lower scattering ratio. We performed calculations in which the ozone column below 40 km was increased by factors of 1.5 and 2.0. In the region of maximum ozone absorption, ~255 nm, little change is observed in the scattering ratio. At larger and shorter wavelengths, 255 ± 40 nm, the scattering ratio decreases. But in the Schumann-Runge bands and above 300 nm the differences remain constant or increases. The best overall agreement was obtained using the original model atmosphere, as given in Table 1.

Angular averaging. *HM* assumed that the scattered ra-

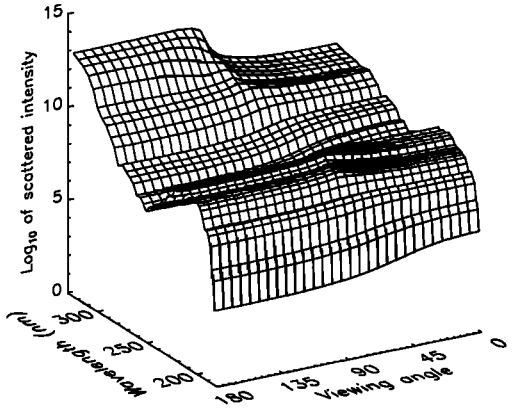

Fig. 4. The modeled scattered solar radiation as a function of wavelength and viewing angle. The wavelength resolution is as in *WMO* [1986] and the angular resolution is 6°. As in Figure 3, the viewing angle is relative to the vertical with $\theta = 0°$ being the zenith direction. The scattered radiation is shown in the plane of the incident solar radiation and the vertical.

diation changes monotonically with θ between the measurement directions. To find the intensities at intermediate angles, they used logarithmic interpolation and then integrated over 4π to obtain the total scattered radiation at 40 km. In Figure 5 of *HM* the scattered radiation is shown for four of the six viewing directions. In Figure 3 of the present paper we show similar modeled intensities. Furthermore, in Figure 4 is shown the variation of the scattered intensity with wavelength and viewing angle. For certain wavelength regions, in particular those where multiple scattering is weak, the scattered intensity may vary by several orders of magnitude with the viewing direction. For all of the four viewing directions displayed in Figure 3 there is good agreement between measurement and theory, except for the Schumann-Runge bands. We note that the largest discrepancies between the modeled and the measured scattering ratios are found in the regions of the spectrum where the intensities vary the least among the different viewing directions (210–230 nm and 280–300 nm). We find this somewhat surprising because one would expect the interpolation between the different viewing directions to be more reliable when the variation among them is the smallest.

4. Conclusion

We have compared the ratio of the scattered to the direct radiation at 40 km, as measured by the SABE 1 experiment with results from state of the art radiative transfer models, including multiple scattering. Between 210 and 300 nm the models predict more scattering than the measurement. No plausible explanation for this lack of agreement is found. Furthermore, in the Schumann-Runge bands the model predicts too little scattering. We note that the measured direct and scattered radiation have different spectral shapes in the Schumann-Runge region (compare Figures 5 and 12 of *HM*).

To help validate radiative transfer models for a Rayleigh-scattering atmosphere as well as increase our confidence in radiation schemes used in photochemical models, further measurements of both the direct and the scattered radiation at a variety of altitudes and zenith angles for clear sky conditions are desirable.

Acknowledgments. One of us, A. K., would like to thank "Gutan på taket" for their hospitality during a stay at the Auroral Observatory, University of Tromsø, Norway. We would like to thank two anonymous referees for their constructive comments. This work was in part supported by the Norwegian Council on Science and Technology and the National Aeronautics and Space Administration through grant NAGW-1265 to the University of Alaska.

References

Allen, M., and J. E. Frederick, Effective photodissociation cross sections for molecular oxygen and nitric oxide in the Schumann-Runge bands, *J. Atmos. Sci.*, *39*, 2066, 1982.

Anderson, D. E., Jr., and S. A. Lloyd, Polar twilight UV-visible radiation field: Perturbations due to multiple scattering, ozone depletion, stratospheric clouds, and surface albedo, *J. Geophys. Res.*, *95*, 7429–7434, 1990.

Anderson, D. E., Jr., and R. R. Meier, The effects of anisotropic multiple scattering on solar radiation in the troposphere and stratosphere, *Appl. Opt.*, *18*, 1955, 1979.

Frederick, J. E., and J. E. Mentall, Solar irradiance in the stratosphere: Implications for the Herzberg continuum absorption of O_2, *Geophys. Res. Lett.*, *9*, 461–464, 1982.

Herman, J. R., and J. E. Mentall, The direct and scattered solar flux within the stratosphere, *J. Geophys. Res.*, *87*, 1319–1330, 1982.

Kylling, A., Radiation transport in cloudy and aerosol loaded atmospheres, Ph.D. thesis, Univ. of Alaska-Fairbanks, 1992.

Lary, D. J., and J. A. Pyle, Diffuse radiation, twilight, and photochemistry, II, *J. Atmos. Chem.*, *13*, 393–406, 1991.

Luther, F. M., and R. J. Gelinas, Effect of molecular multiple scattering and surface albedo on atmospheric photodissociation rates, *J. Geophys. Res.*, *81*, 1125–1132, 1976.

Meier, R. R., D. E. Anderson, Jr., and M. Nicolet, Radiation transfer in the troposphere and stratosphere from 240–1000 nm, I, General analysis, *Planet. Space Sci.*, *33*, 923, 1982.

Molina, L. T., and M. J. Molina, Absolute absorption cross sections of ozone in the 185- to 350-nm wavelength range, *J. Geophys. Res.*, *91*, 14,501–14,508, 1986.

Nicolet, M., On the molecular scattering in the terrestrial atmosphere: An empirical formula for its calculation in the homosphere, *Planet. Space Sci.*, *32*, 1467–1468, 1984.

Shardanand, and A. D. Pradad Rao, Collision-induced absorption of O_2 in the Herzberg continuum, *J. Quant. Spectrosc. Radiat. Transfer*, *17*, 433–439, 1977.

Shettle, E. P., Models of aerosols, clouds and precipitation for atmospheric propagation studies, paper presented at AGARD Conference 454 on Atmospheric Propagation in the UV, Visible, IR and Millimeter Region and Related System Aspects, Advis. Group for Aeronaut. Res. and Dev., Copenhagen, Oct. 9–13, 1989.

Stamnes, K., On the computation of the angular distribution of radiation in planetary atmospheres, *J. Quant. Spectrosc. Radiat. Transfer*, *28*, 47, 1982.

Stamnes, K., S.-C. Tsay, W. Wiscombe, and K. Jayaweera, Numerically stable algorithm for discrete-ordinate-method radiative transfer in multiple scattering and emitting layered media, *Appl. Opt.*, *27*, 2502, 1988.

World Meteorological Organization (WMO), Atmospheric ozone 1985, Assessment of our understanding of the processes controlling its present distribution and changes, *Rep. 16*, Global Ozone Res. and Monit. Proj., Geneva, 1986.

D. E. Anderson, The Johns Hopkins University, Applied Physics Laboratory, Johns Hopkins Road, Laurel, MD 20723-6099.

A. Kylling and K. Stamnes, Geophysical Institute, University of Alaska-Fairbanks, Fairbanks, AK 99775-0800.

R. R. Meier, E. O. Hulburt, Center for Space Research, Space Science Division, Naval Research Laboratory, Washington, D. C. 20375.

(Received May 22, 1992;
revised October 27, 1992;
accepted November 6, 1992.)